4. The mass balance is strongly negative for active ice streams but positive for Ice Stream C, which stopped streaming about 150 years ago. The overall mass balance for the Ross Embayment is about -23 ± 15 km^3 year^{-1}, which corresponds to an average surface lowering of 27 ± 21 mm year^{-1} [S. Shabtaie and C. R. Bentley, *J. Geophys. Res.* **92**, 1311 (1987)]. The large uncertainty arises because mass balance is the difference between two large numbers, each with large uncertainties; the few available point measurements of accumulation and thinning show large spatial variability.
5. D. R. MacAyeal, *Nature* **359**, 29 (1992); R. B. Alley and I. M. Whillans, *Science* **254**, 959 (1991).
6. R. Retzlaff and C. R. Bentley, *J. Glaciol.* **39**, 495 (1993); R. Jacobel, T. Scambos, C. Raymond, A. Gades, *J. Geophys. Res.* **101**, 5499 (1996); C. R. Bentley, *J. Glaciol.* **44**, 157 (1998).
7. B. L. Hall, G. H. Denton, C. H. Hendy, *Geograf. Ann.*, in press.
8. B. L. Hall and G. H. Denton, *ibid.*, in press; J. M. Clayton-Greene, C. H. Hendy, A. C. Hogg., *N. Z. J. Geol. Geophys.* **31**, 353 (1988); M. A. Dagel, thesis, University of. Maine, Orono (1989).
9. Unless otherwise stated, all ages in the text are in calendar years. Carbon-14 ages were obtained from accelerator mass spectrometry (AMS) or from conventional counting. P. T. Doran *et al.* [*Palaeogeogr. Palaeoclimatol. Palaeoecol.* **147**, 223 (1999] showed that ^{14}C dates of algae from lake-edge deposits in the dry valleys do not suffer from a substantial reservoir effect. Dates of marine materials were corrected by 1300 years for the marine reservoir effect [P. A. Berkman and S. L. Forman, *Geophys. Res. Lett.* **23**, 363 (1996)]. Corrected ^{14}C ages were converted to calendar years with algorithms of M. Stuiver *et al.* [*Radiocarbon*, **40**, 1041 (1998)] and E. Bard [*Geochim. Cosmochim. Acta* **62**, 2025 (1998)].
10. B. L. Hall and G. H. Denton, *J. Quat. Sci.*, in press.
11. W. R. Peltier, *Rev. Geophys.* **36**, 603 (1998); A. M. Tushingham and W. R. Peltier, *J. Geophys. Res.* **96**, 4497 (1991); W. R. Peltier, *Quat. Res.* **29**, 93 (1988).
12. D. R. Marchant, G. H. Denton, T. M. Dochat, *Geograf. Ann.*, in press.
13. J. G. Bockheim, G. H. Denton, B. G. Anderson, M. Stuiver, *Quat. Res.* **31**, 229 (1989).
14. Our conceptual model invokes northward or westward flow of thick WAIS ice across Roosevelt Island during glacial times. During deglaciation, the thicker ice in the deep surrounding troughs underwent more rapid strain thinning than did the relatively shallow ice of Roosevelt Island, producing first a N-S ridge and then an isolated dome.
15. Variations of ice thickness and internal stratigraphy were measured from radio echo-sounding traverses with a center frequency of 7 MHz, which corresponds to a wavelength of ~20 m in ice. Surface velocities and topography were measured by repeat surveys of poles with the Global Positioning System. Accumulation rate was estimated from stratigraphic profiles in three 2-m snow pits and from beta activity of three 16-m cores analyzed by J. Dibb (University of New Hampshire). Spikes in beta activity represent horizons deposited in 1955 and 1965; the depth of the horizon, together with measurements of the firn density profile, was used to calculate the average accumulation rate.
16. C. F. Raymond, *J. Glaciol.* **29**, 357 (1983).
17. D. G. Vaughan, H. F. J. Corr, C. S. M. Doake, E. D. Waddington, *Nature* **398**, 323 (1999).
18. The model followed layers as they moved downward under the ice divide and under a flank. The two ice flow regimes were represented with three parameters: the downward velocity at the surface and two fractional heights above the bed, h_{divide} and h_{flank}, at which the downward velocity profile changes from quadratic to linear on the divide and flanks [W. Dansgaard and S. J. Johnsen, *J. Glaciol.* **8**, 215 (1969)]. A finite element model (*16*), constrained by our measured surface and bed topography, guided the choice of values for h_{divide} and h_{flank}.
19. Ice cap thinning results from an imbalance between accumulation and the downward velocity at the surface and was calculated from $\dot{H} = \dot{b} - \nabla \cdot Q$, where $\dot{H}$ is the thinning rate, $\dot{b}$ is the ice equivalent accumulation rate, and $\nabla \cdot Q$ is the horizontal flux divergence [L. A. Rasmussen, *J. Glaciol.* **31**, 115 (1985)]. The flux divergence comes from measurements of ice thickness H and the divergence of the horizontal surface velocity $\nabla \cdot U_s$; that is, $\nabla \cdot Q = \gamma H \nabla \cdot U_s$. The parameter γ varies from about 0.8 in the case of no sliding with flow dominated by bed-parallel shear to 0.6 as might occur beneath a nonsliding divide (*16*). Analysis of pole positions surveyed during the early 1960s [J. L. Clapp, *Univ. Wisconsin Res. Rep. 65-1* (1965)] indicates that $\nabla \cdot U_s$ at the summit of Roosevelt Island is $\sim 5.1 \times 10^{-4}$ year^{-1}, which, for $\dot{b} = 0.18$ m year^{-1}, implies thinning by 0.06 to 0.11 m year^{-1}.
20. Bedrock beneath Roosevelt Island is ~200 m below present-day sea level (Fig. 3), and the surrounding trough is about 500 m below sea level. If ice surrounding the island was floating (requiring ice <560 m thick, or less if sea level was lower), and the ice surface across the island was flat (no dome), then ice on the island would have to be ~260 m thick. This is unlikely because it requires thickening of ~460 m to achieve present morphology; this conflicts with the continuity analysis (*19*) and with the pattern of bumps beneath the divide (Fig. 3), both of which imply thinning.
21. C. Baroni and G. Orombelli, *Quat. Res.* **36**, 157 (1991).
22. _____, *Geology* **22**, 23 (1994).
23. R. H. Fillon, I. A. Hardy, F. J. E. Wagner, J. T. Andrews, H. W. Josenhans, *Current Res. Part B Geol. Surv. Can. Pap.* **81-1B**, 105 (1981); E. W. Domack, A. J. T. Jull, J. B. Anderson, T. W. Linick, C. R. Williams, *Quat. Res.* **31**, 277 (1989); P. T. Harris, P. E. O'Brien, P. Sedwick, E. M. Truswell, *Pap. Proc. R. Soc. Tasmania* **130**, 47 (1996).
24. J. T. Andrews *et al.*, *Quat. Res.* **52**, 206 (1999); K. J. Licht, W. L. Cunningham, J. T. Andrews, E. U. Domack, A. E. Jennings, *Polar Res.* **17**, 203 (1998).
25. D. L. Morse, E. D. Waddington, E. J. Steig, *Geophys. Res. Lett.* **25**, 3383 (1998).
26. Changes in global sea level have been inferred from elevations and ages of drowned reefs in the Caribbean-Atlantic region and Tahiti [R. G. Fairbanks, *Nature* **342**, 637 (1989); E. Bard *et al.*, *ibid.* **382**, 241 (1996); P. Blanchon and J. Shaw, *Geology* **23**, 4 (1995)].
27. Postglacial models of West Antarctica predict uplift of ~5 mm year^{-1} [T. S. James and E. R. Ivins, *J. Geophys. Res.* **103**, 4993 (1998)]. Figure 2 suggests that RSL has decreased ~4 mm year^{-1} over the past 7500 years.
28. J. Weertman, *J. Glaciol.* **13**, 3 (1974).
29. R. H. Thomas, S. N. Stephenson, R. A. Bindschadler, S. Shabtaie, C. R. Bentley, *Ann. Glaciol.* **11**, 8 (1988).
30. Comparison of declassified satellite photography taken with more recent images shows that the ridge between Ice Streams B and C has eroded 14 km and that Ice Stream B has widened 4 km in the 29 years between measurements [R. A. Bindschadler and P. Vornberger, *Science* **279**, 689 (1998)].
31. Collapse of the WAIS has been inferred from high stands of sea level in the past [J. H. Mercer, *Nature* **271**, 321 (1978)] and the discovery of young diatoms and high concentrations of ^{10}Be beneath parts of the WAIS that are now grounded [R. P. Scherer *et al.*, *Science* **281**, 82 (1998)]. B. L. Hall and G. H. Denton [*Antarct. J. U.S.* **31**, 78 (1996)] suggested that the grounding line receded from McMurdo Sound to its present position in Holocene time and that retreat might continue back into the interior reservoir of the WAIS. R. Bindschadler [*Science* **282**, 428 (1998)] calculated the time of complete deglaciation by assuming that the grounding line will continue to retreat to the divide at the average rate.
32. T. B. Kellogg, D. E. Kellogg, M. Stuiver, in *Contributions to Antarctic Research I*, vol. 50 of Antarctic *Research Series*, D. H. Elliot, Ed. (American Geophysical Union. Washington, DC, 1990), pp. 25–56.

33. This work was funded by the NSF through Office of Polar Program grants 9118678, 9420648, and 9615347. Carbon-14 samples were processed at the NSF-Arizona AMS facility and at the University of Washington. We thank R. Ackert, B. Andersen, C. Bentley, J. Bockheim, M. Conway, R. Kelly, N. Lord, T. Lowell, N. Nereson, B. Overturf, B. Smith, M. Stuiver, and S. Wilson for valuable contributions. G.H.D. had the idea to study the future of the West Antarctic Ice Sheet by examining its past. B.L.H. and G.H.D collected and interpreted the geologic and ^{14}C data. A.M.G. and H.C. collected and interpreted the geophysical data from Roosevelt Island. E.D.W. conceived and implemented the internal layer evolution model. B.L.H. and H.C. wrote the report.

21 May 1999; accepted 23 August 1999

Tributaries of West Antarctic Ice Streams Revealed by RADARSAT Interferometry

Ian Joughin,[1]* Laurence Gray,[2] Robert Bindschadler,[3] Stephen Price,[4] David Morse,[5] Christina Hulbe,[3] Karim Mattar,[2] Charles Werner[1]

Interferometric RADARSAT data are used to map ice motion in the source areas of four West Antarctic ice streams. The data reveal that tributaries, coincident with subglacial valleys, provide a spatially extensive transition between slow inland flow and rapid ice stream flow and that adjacent ice streams draw from shared source regions. Two tributaries flow into the stagnant ice stream C, creating an extensive region that is thickening at an average rate of 0.49 meters per year. This is one of the largest rates of thickening ever reported in Antarctica.

The West Antarctic Ice Sheet, which would raise sea level by 5 to 6 m if it melted, has been a subject of intense glaciological study since doubts about its stability were first raised (*1*). Unlike the Greenland Ice Sheet and most of the East Antarctic Ice Sheet, much of the West Antarctic Ice Sheet is grounded below sea level and underlain by marine sediments. When saturated with water (*2*), these sediments may affect the dynamics of ice motion by allowing fast movement. Although the possibility of a catastrophic collapse of the ice sheet is under debate (*3*), field and satellite observations have established that substantial changes are occurring in West Antarctica (*4*–*6*), particularly in the ice streams.

Theoretical arguments (*7*) and inferred results (*8*) predict that the onsets of the ice streams feeding the Ross Ice Shelf are migrating inland at rates of several hundred meters per year. Regions inland of the onsets, from which ice streams draw mass and inherit thermal and mechanical signatures, are largely unexplored. In our study, we used satellite radar interferometry to provide a broad-scale view of inland ice flow feeding into four West Antarctic ice streams.

Satellite radar interferometry (*9*) has become a well-established method for measuring ice motion. Unfortunately for Antarctic studies, all past and present civilian synthetic aperture radars were designed to fly with the instrument pointed north, so that areas south of 79°S, including much of West Antarctica, are not imaged. In September 1997, however, the Canadian RADARSAT satellite (*10*) was maneuvered to point toward the south for a period of 30 days in order to perform high-resolution mapping of the complete Antarctic continent (*11*).

The 24-day repeat period of RADARSAT provides an interferometric data set that is well suited for measuring the relatively slow (<100 m/year) motion of ice flowing toward the ice streams. Direct interferometric measurements in the faster moving areas, such as the main trunks of the ice streams, are more difficult because the large displacements occurring over the 24-day repeat period cause phase aliasing and decorrelation. In faster areas, vector ice displacements occurring between a pair of precisely coregistered radar images were determined through "speckle tracking," although with lower resolution and poorer accuracy (*12*). In addition, a combination of interferometry and speckle tracking was used to achieve vector estimates in areas where observations from only a single direction were available.

We used data from the RADARSAT Antarctic Mapping Mission to produce a surface velocity map (*13*) of most of the region flowing into ice streams B, C, D, and E in West Antarctica (Fig. 1). Most of the area mapped in Fig. 1 lacks visible features, such as crevasses, required for feature tracking with optical imagery (*14*); interferometric methods are free of such requirements. In situ velocity measurements (Fig. 1) are sparse and irregularly spaced (*15*), so that, with the exception of the regular grid in the upstream region of ice stream D (*16*), they do not reveal spatial patterns of flow. These data, however, provide an important source of control for our velocity field. Our interferometric velocity data increase the number of velocity measurements in regions upstream of the ice streams by several orders of magnitude.

The data (Fig. 1) show that individual ice streams are fed by multiple tributaries and that source areas are shared. Ice stream E receives ice from two tributaries that share the same upstream reservoir as a major tributary to ice stream D. The other major tributary that feeds D, previously identified and mapped through a field campaign (*16*), originates from the same source area as a previously unknown major tributary leading to ice stream C. Much of the southern tributary of ice stream C draws ice from close to the head of ice stream B.

Previous calculations of ice stream mass balance assigned distinct catchment basins to individual ice streams (*17, 18*). Shared source regions complicate the delineation of adjacent ice stream catchment areas and the calculation of individual ice stream mass balances. Moreover, shared source regions make it more likely that the relative contributions to neighboring ice streams change over time.

Ice streams have been mapped by a combination of visible and radar imagery and by radio echo sounding (*18–20*). Our results show that, upstream of the previously mapped ice streams, there exists a network of tributaries extending far into the ice sheet interior. Tributary speeds are faster than that of the surrounding ice, yet the speed contrast is too small to generate crevassed margins. The transition to an ice stream with crevassed margins takes place at a speed of ~100 m/year. Short isolated sections of this network have been identified before (*21, 22*), but Fig. 1 shows the intricate nature of the flow network inland of the ice streams. Speeds within the tributaries are nearly an order of magnitude faster than that of the surrounding ice. It is probable that the distinct dynamics of ice

[1]Jet Propulsion Laboratory, California Institute of Technology, M/S 300-235, 4800 Oak Grove Drive, Pasadena, CA 91109, USA. [2]Canada Centre for Remote Sensing, Applications Division, 588 Booth Street, Ottawa, Ontario K1A 0Y7, Canada. [3]Code 971, Oceans and Ice Branch, NASA/Goddard Space Flight Center, Greenbelt, MD 20771, USA. [4]SAIC General Sciences Corporation, 4600 Powder Mill Road, Beltsville, MD 20705–2675, USA. [5]Institute for Geophysics, University of Texas at Austin, 4412 Spicewood Springs Road #600, Austin, TX 78759, USA.

*To whom correspondence should be addressed. E-mail: ian@radar-sci.jpl.nasa.gov

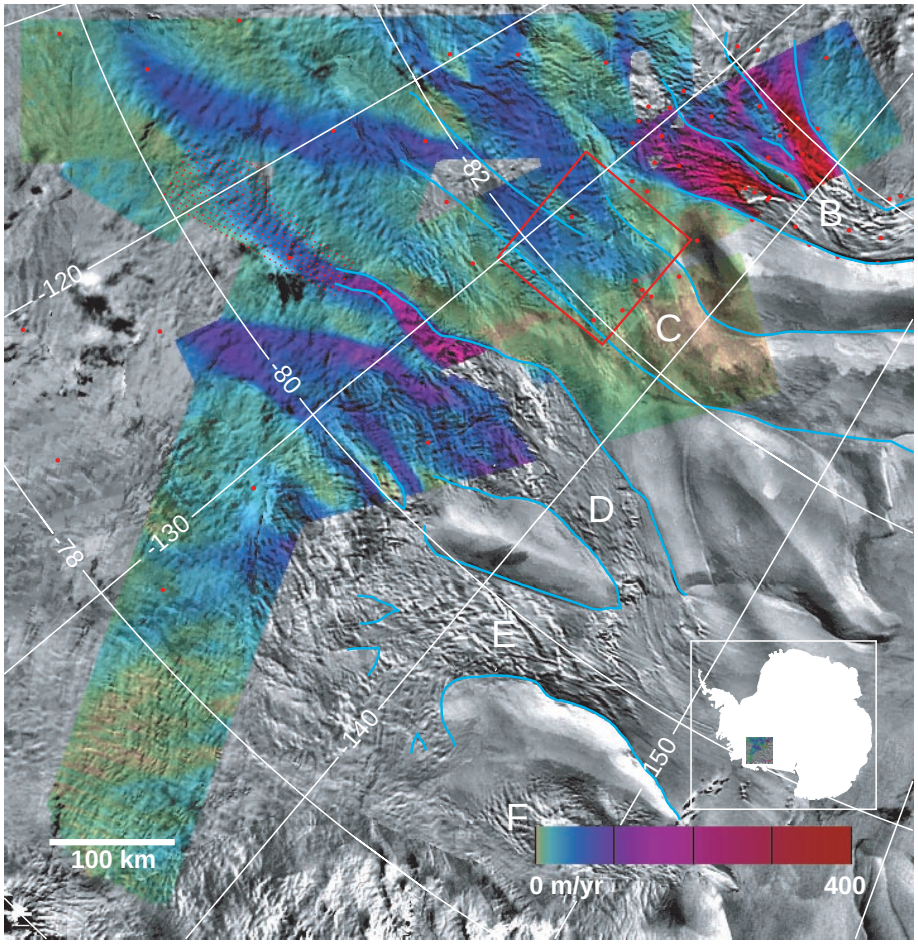

Fig. 1. Ice flow speed determined from multiple swaths of RADARSAT Antarctic Mapping Mission data (*13*) coregistered with a mosaic of advanced very high resolution radiometer imagery. Ice flow is generally from top left to bottom right. The red dots show the locations of in situ velocity measurements used for control, with small red dots corresponding to the survey grid mentioned in the text (*16*). The red box indicates the locations of data shown in Fig. 4. Blue lines show previously mapped ice stream margins (ice streams are indicated by letter). m/yr; meters per year.

streams coincides roughly with the formation of crevassed margins and that the dynamics within the tributary network upstream of the ice streams represents a combination of internal deformation and basal sliding.

The tributary network coincides with valleys in the subglacial topography (Fig. 2), with the correspondence being much stronger for the tributaries than for the ice streams (*23*). The tributaries are guided by and contained within subglacial valleys, and only rarely does ice flow cross a ridge between valleys. The deepest subglacial valley, called the Bentley Subglacial Trench (Fig. 2), is over 2500 m below sea level. Within this trench, a long wide tributary begins that feeds the northern tributary of ice stream C and the southern tributary of ice stream D. The faster flow in this trench is probably due to the fact that this ice is nearly twice as thick as the adjacent ice (*24*).

Relative differences in ice thickness in and adjacent to other subglacial valleys are not as large as those for the Bentley Trench. Thus, other processes are likely involved in the flow of those tributaries. In a region where accumulation and geothermal heat flux are constant, thicker ice will be warmer near the base, making the ice softer and more deformable, but this effect in combination with the larger ice thickness may not be sufficient to explain the larger speeds in other tributaries. Subglacial valleys are also expected to have collected sediment during times when the ice was absent, as well as the subglacial water formed from geothermal heating and basal friction. Because subglacial water and sediment are necessary for streaming flow, it is possible that they also contribute in some measure to tributary flow (*21*).

Ice streams D and E form in a broad low-relief basin (Fig. 3) and are fed by a network of narrow tributaries 10 to 20 km wide. Several features of the D and E regions stand out. First, most of the basin feeds ice stream E (*18*). Second, the southern tributaries of E and the northern tributaries of D diverge from one upstream source to become a network of features narrower than the coalescing tributaries seen elsewhere. Figure 2 shows that this network conforms to relatively narrow valleys in the subglacial topography. Although these tributaries and the downstream portions of D and E are clearly separated from each other by bedrock ridges, they are joined in the tributary region. Third, the pattern of speed (Figs. 1 and 3) shows alternating acceleration and deceleration as tributary ice flows toward ice streams D and E.

In contrast to ice streams D and E, observations and modeling studies have suggested that ice streams B and C are linked (*19, 25*), possibly because the bedrock topography between the two ice streams is relatively sub-

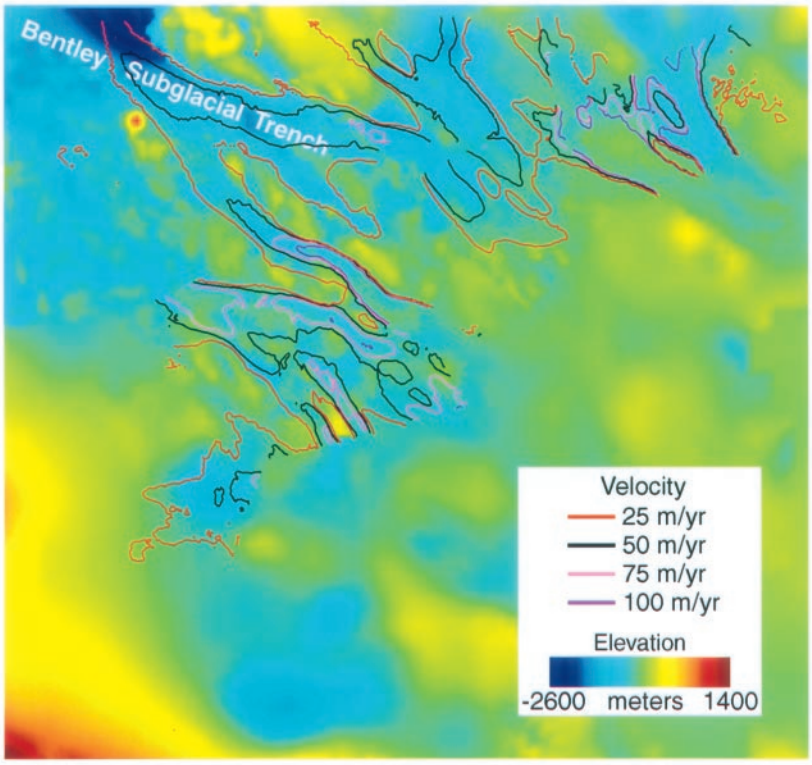

Fig. 2. Ice speeds up to 100 m/year contoured over bed topography. The area shown is approximately the same as in Fig 1. Basal topography is the difference between ice sheet surface elevation (*30*) and ice thickness from a number of sources (*29–31*), resulting in a bed map with spatially varying resolution.

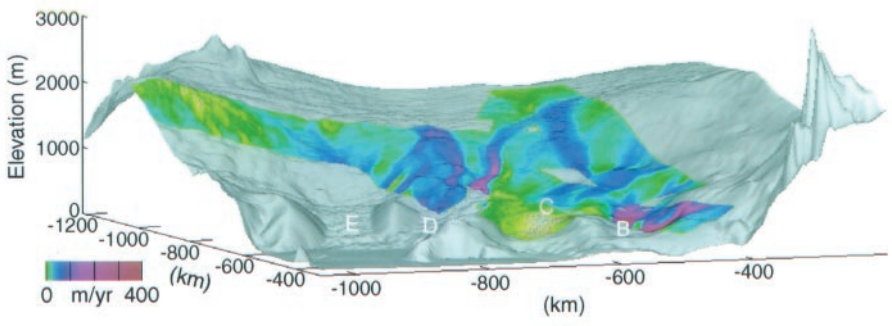

Fig. 3. Ice speed superimposed on surface elevation. View is upstream from the Ross Ice Shelf toward the inland ice divide. A section of the Transantarctic Mountains appears on the right. The origin is at the South Pole.

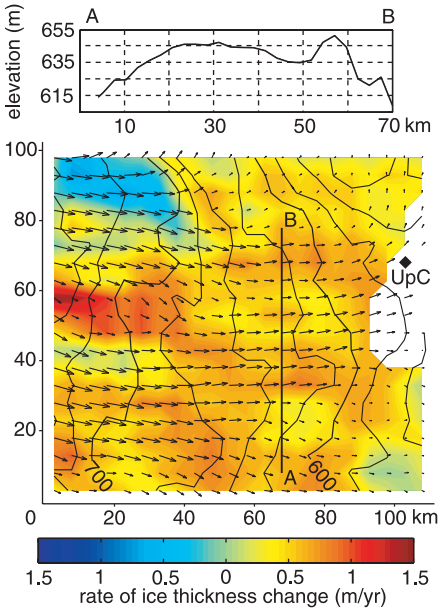

Fig. 4. (**Top**) Surface elevation along profile line A–B. (**Bottom**) Rate of ice thickness change (colors), surface elevation (contour lines), and flow direction over the box outlined in Fig. 1 (right edge corresponds to downstream edge in Fig. 1). Elevation contour interval is 25 m. Vector length is proportional to ice speed. Location of the Upstream C (UpC) camp is marked. White area at the right-hand edge of the bottom panel is due to a small gap in velocity data that is enlarged through subsequent calculations.

dued (Fig. 2). Although ice stream B currently discharges ~50% more ice than it accumulates over its catchment area (*17, 18*) and discharge from neighboring ice stream C is negligible (*18*), their combined discharges approximately balance their combined accumulation. Figures 1 and 3 show that the southern tributary to ice stream C cuts across the heads of the much shorter northern tributaries feeding ice stream B. This suggests that there is a limited area from which ice stream B can continue to draw ice without interacting with the northern tributary now flowing into ice stream C.

Although there are two active tributaries flowing into the head of ice stream C, the main body of the ice stream is known to have ceased rapid motion ~140 years ago (*26*). Thus, the boundary region between the active tributaries and the formerly streaming portion of the ice stream must be thickening over time. The mean thickening rate over the red box in Fig. 1 is 0.49 ± 0.02 m/year (Fig. 4, bottom) (*27*). This thickening rate agrees well with an independent in situ measurement of 0.56 m/year obtained at the Upstream C camp (Fig. 4, bottom) (*28*).

The thickening in this region is probably responsible for the formation of the 70-km-wide bulge discernible in the surface elevations (Fig. 4, top). Slightly higher thickening rates at the bulge's perimeter (approximately delineated by the 575-m elevation contour in Fig. 4, bottom), suggest that the bulge is spreading slowly. Because active ice streams generally have lower surface elevations than the adjacent ice, this bulge probably has thickened more than its average height of 25 m above a horizontal datum. If the area now occupied by the bulge was depressed by a mean of 45 m below the adjacent ice when ice stream C stopped, the present flow field and the associated thickening rates would have formed a bulge with the observed volume. A depression of this magnitude is feasible on the basis of a comparison with active ice streams [for example, tributary B2, adjacent to the thickening portion of ice stream C (*29*)]. Thus, it is possible that the tributary flow of ice stream C has persisted despite the stagnation of the ice stream.

In the blue area of Fig. 4 (bottom) is an area thinning at a mean rate of 1 m/year. Examination of the flow pattern shows that ice in this region is diverging strongly as some ice continues to flow along ice stream C, and neighboring ice turns nearly 90° to flow into the northernmost branch of ice stream B (Fig. 4). This appears to be an evolving encroachment of ice stream B on C. Despite the high thinning rate, no expression of this pattern is seen in the surface elevations, suggesting that this encroachment is more recent than the stagnation of ice stream C.

Overall, the data show that long tributaries, flowing much faster than the surrounding ice, form an extensive network, delivering ice to the ice streams. These tributaries coincide with valleys in the subglacial floor where sediments, subglacial water, and warmer ice are expected to concentrate. Many tributaries emanate from common source areas, complicating the notion of distinct catchments. The discovery of this tributary network and its speeds establishes that the transition from slow inland flow to fast ice stream flow occurs gradually, over an extended distance.

References and Notes

1. J. Weertman, *J. Glaciol.* **13**, 3 (1974).
2. R. B. Alley, D. D. Blankenship, C. R. Bentley, S. T. Rooney, *Nature* **322**, 57 (1986).
3. M. Oppenheimer, *ibid.* **393**, 325 (1998).
4. R. Bindschadler and P. Vornberger, *Science* **279**, 689 (1998).
5. E. J. Rignot, *ibid.* **281**, 549 (1998).
6. D. J. Wingham, A. J. Ridout, R. Scharroo, R. J. Arthern, C. K. Shum, *ibid.* **282**, 456 (1998).
7. R. B. Alley and I. M. Whillans, *ibid.* **254**, 959 (1991).
8. R. A. Bindschadler, *Ann. Glaciol.* **24**, 409 (1997); *Science* **282**, 428 (1998); S. Price and I. Whillans, unpublished material.
9. R. M. Goldstein, H. Engelhardt, B. Kamb, R. M. Frolich, *Science* **262**, 1525 (1993).
10. The Canadian RADARSAT satellite and program are described in the special RADARSAT issue of *Can. J. Remote Sensing* **19** (no. 4) (1993).
11. RADARSAT collected data in south-looking mode over Antarctica during the period from 19 September to 20 October 1997. See work by K. C. Jezek *et al.*, paper presented at the International Geoscience and Remote Sensing Symposium (IGARSS) '98, Seattle, WA, 6 to 10 July 1998; K. C Jezek, *Report 17* (Byrd Polar Research Center, Ohio State University, Columbus, 1998).
12. A technique for determining two-dimensional ice motion from one pair of coherent images was presented by K. H. Thiel, A. Wehr, X. Wu, paper presented at the Workshop on Glaciological Applications of Satellite Radar Interferometry, Pasadena, CA, 28 to 29 March 1996. Rignot (*5*) also used a related correlation technique for two-dimensional motion and refers to R. Michel (thesis, University of Paris XI, 1997). Independently, we have developed the speckle-tracking approach (A. L. Gray *et al.*, paper presented at IGARSS '98, Seattle, WA, 6 to 10 July 1998), which takes advantage of its ability to coregister members of an interferometric pair with subpixel accuracy to quantify two-dimensional motion.
13. Interferometric phase data were used to obtain velocities at which the phase data could be unwrapped (for example, <125 m/year). Phase unwrapping refers to the process by which the modulo-2 ambiguity in the phase data is removed. Where crossing swaths were available, both horizontal vector components were derived from the phase data [I. Joughin, R. Kwok, M. Fahnestock, *IEEE Trans. Geosci. Remote Sensing* **36**, 25 (1998)]. In regions with only single-track coverage, speckle tracking was used for the along-track component. Speckle tracking was used for both components where displacements were too large to allow phase unwrapping. A small gap in the RADARSAT coverage was filled with the data from the survey grid in Fig. 1 (*16*). Velocity measurements (see Fig. 1) (*15*) were used to solve for the interferometric baseline parameters. The residual difference between control points and estimated velocity is 5 m/year, indicative of the random component of the velocity error. Systematic errors may be higher in areas that are not well constrained by the control velocities.
14. R. A. Bindschadler and T. A. Scambos, *Science* **252**, 242 (1991); T. A. Scambos, M. J. Dutkiewicz, J. C. Wilson, R. A. Bindschadler, *Remote Sensing Environ.* **42**, 177 (1992).
15. Data were provided by the EOS Distributed Active Archive Center at the National Snow and Ice Data Center, University of Colorado, Boulder, CO (available at www-nsidc.colorado.edu/NSIDC/ANTARCT_VELOC/).
16. X. Chen, R. A. Bindschadler, P. L. Vornberger, *Surv. Land Inf. Syst.* **58**, 247 (1998).
17. I. M. Whillans and R. A. Bindschadler, *Ann. Glaciol.* **11**, 187 (1988).
18. S. Shabtaie and C. R. Bentley, *J. Geophys. Res.* **92**, 1311 (1987).
19. K. E. Rose, *J. Glaciol.* **24**, 63 (1979).
20. R. Bindschadler and P. Vornberger, *Eos Trans. Am. Geophys. Union* **17**, 741 (1990); T. A. Scambos and R. Bindschadler, *Antarct. J. U.S.* **26**, 312 (1991).
21. R. E. Bell *et al.*, *Nature* **394**, 58 (1998); S. Anandakrishnan, D. D. Blankenship, R. B. Alley, P. L. Stoffa, *ibid.*, p. 62.
22. S. M. Hodge and S. K. Doppelhammer, *J. Geophys. Res.* **101**, 6669 (1996); S. N. Stephenson and R. A. Bindschadler, *Ann. Glaciol.* **14**, 273 (1990).
23. C. R. Bentley, *J. Geophys. Res.* **92**, 8843 (1987).
24. With surface slope, temperature, and crystal fabric remaining constant, ice speed increases as the fourth power of ice thickness. A twofold increase in ice thickness can account for a 16-fold increase in speed. Calculations of deformational velocity at several locations within the trench using a flow rate factor of 10^{-16} $year^{-1}$ Pa^{-3} are similar to the measured velocity.
25. R. B. Alley, S. Anandakrishnan, C. R. Bentley, N. Lord, *Ann. Glaciol.* **20**, 187 (1994); A. J. Payne, *Geophys. Res. Lett.* **25**, 3173 (1998).
26. R. Retzlaff and C. R. Bentley, *J. Glaciol.* **39**, 553 (1993).
27. Our velocity data and the ice thickness data from the University of Wisconsin are on a 5-km grid. The change in ice thickness at grid center points is calculated as the residual flux into each grid cell divided by the area of the grid cell, plus a uniform accumulation rate of 0.09 m/year [E. R. Venteris and I. M. Whillans, *Ann. Glaciol.* **27**, 227 (1998)]. Error propagation gives 1σ uncertainties in the rates of thickness change between 0.35 and 0.67 m/year. The 1σ uncertainty in the mean rate of thickness change is smaller (0.02 m/year). Additional uncertainty arises from the assumption that surface velocity is equal to the depth-averaged velocity. For nonsliding regions (speeds less than ~15 m/year), this can overestimate the thickness change by up to 20%. Measured surface velocities suggest substantial sliding for most of the calculation area, in which case depth-averaged and surface velocities are equal, and the overestimation in thickness change is negligible.
28. G. Hamilton and I. M. Whillans, personal communication.
29. R. Retzlaff, N. Lord, C. R. Bentley, *J. Glaciol.* **39**, 495 (1993).
30. J. L. Bamber and R. A. Bindschadler, *Ann. Glaciol.* **25**, 439 (1997).
31. D. Blankenship, unpublished data.

32. I.J. and C.W. performed this work at the Jet Propulsion Laboratory under contract with NASA; K.M. is under contract from Intermap Technologies (Calgary, Alberta, Canada). R.B. and S.P were supported by NASA grant NRA-98-OES-03, D.M. was supported by NSF grant OPP-9319369, C.H. was supported by a NRC Resident Research Associateship, and L.G. and K.M. were supported by the Canada Centre for Remote Sensing. RADARSAT data are copyrighted by the Canadian Space Agency. We thank J. Bamber, C. Bentley, and D. Blankenship for the surface and bed elevation data; P. Vornberger for the digitized ice stream boundaries shown in Fig. 1; and C. Bentley and R. Alley for comments that led to substantial improvements to this report.

15 June 1999; accepted 9 August 1999